Int. J. Electrochem. Sci., 13 **(2018)** 11526 – 11538, doi: 10.20964/2018.12.11

International Journal of
ELECTROCHEMICAL
SCIENCE
www.electrochemsci.org

Corrosion characteristic of Cu-10Ni-Fe_x in 3.5 % NaCl

Rongwei Zhang, Zhiyun Zhu[*]*, Xiang Leng, Jie Pan, Yinghui Zhang*[*]

School of Material Science and Engineering, Jiangxi University of Science and Technology, Ganzhou 341000,China
[*]E-mail: zhiyunzhu@126.com, jxustzyh@163.com

Received: 8 August 2018 / *Accepted:* 13 September 2018 / *Published:* 5 November 2018

The corrosion charateristic of Cu-10Ni-Fe_x alloys (x=0.84, 1.26, 1.76) in 3.5 % NaCl solution was investigated by using electrochemical impedance spectroscopy, potentiodynamic polarization curve, X-ray Diffraction and X-ray photoelectron spectroscopy. The results showed that the order of corrosion resistance is Cu-10.52Ni-1.26Fe＞Cu-10.44Ni-0.84Fe＞Cu-10.48Ni-1.76Fe. Fe exists in the form of FeOOH and FeO in the product films, whilst Ni exists in the form of NiO, $Ni(OH)_2$, and metallic Ni in the product films. FeOOH promotes the enrichment of the Ni content and the formation of NiO. The product film of Cu-10.52Ni-1.26Fe with the best corrosion resistance contained the highest content of FeOOH. In addition, the mechanism of FeOOH on the corrosion resistance has been discussed.

Keywords: Fe element; corrosion resistance; Cu-Ni alloy; corrosion product film; Electrochemical impedance spectroscopy

1. INTRODUCTION

Copper and its alloys are widely used in marine applications due to excellent biofouling and corrosion resistance [1]. Among the well-known copper alloys, copper-nickel alloysthat contain 5~30 % Ni show superior corrosion resistance compared to the other copper alloys in a marine environment[2]. Generally, the corrosion product films formed on the surface of the copper alloys play a key role for inhibiting future corrosion[3]. During the corrosion process, it has been demonstrated that the Ni element in the copper-nickel alloy would modifies the structure of the barrier passive films by segregating into protective a Cu_2O layer via solid-state reaction[4]. Therefore, Ni improves the corrosion resistance of the copper-nickel alloy. In addition, this effect could be greatly enhanced by several other microalloying elements, such as Fe, Mn, Al, Cr , etc[5-9].

Bailey[10] first suggested that Fe is a beneficial element for improving the corrosion resistance of copper-nickel alloys, which was attributed to a golden, almost transparent, more protective oxide film formed on the surface. In addition, Bailey claimed the optimum Fe content for copper-nickel alloy is Cu-10Ni-2Fe and Cu-30Ni-1Fe. Subsequently, Pearson[11] reported that the Fe addition could increase corrosion resistance of copper-nickel alloy if the Fe were in solid solution. The negative role of high Fe content (>2 %) on the corrosion behaviour of 90Cu-10Ni alloys in chloride solutions was confirmed by Zanoni et al[12]. Therefore, the Fe content in commercial Cu-Ni alloys is generally less than 2 % Fe[11]. Recently, O. Ekerenam reported the difference of component and corrosion behaviour between the 90Cu-10Ni tubes from different manufacturers[13]. However, there still has been no explicit investigation provided for the influence of Fe content on the corrosion product film of Cu-10Ni alloy.

In this paper, three Cu-10Ni-Fe_x alloy samples (Cu-10.44Ni-0.84Fe, Cu-10.52Ni-1.26Fe, Cu-10.48Ni-1.76Fe) were prepared, and the effect of Fe content on the corrosion resistance of Cu-10Ni alloy were investigated by electrochemical impedance spectroscopy and polarization curves in conjunction with characterization of the corrosion products via XRD and XPS.

2. EXPERIMENTAL

2.1 Sample preparation

Three samples, which were preparedby the following steps, were designed to investigate the effect of Fe content on the corrosion behaviour of Cu-10Ni alloy. First, the Cu-10Ni-Fe_x alloys were melted using a vacuum furnace and cast into a mode to make ingots. Second, the cast ingots were hot-rolled to a 3 mm thick plate at 950 °C and then annealed at 720 °C for 1 hour. Subsequently, the samples for corrosion electrochemical test (10×10×2 mm) were prepared by electrical discharge machining followed by grinding, polishing and cleaning with deionized water. The chemical composition of the samples was measured by inductively coupled plasma mass spectrometry (ICP-MS) and the results are listed in Table 1.

Table 1. Chemical composition of the Cu-10Ni-Fe_x alloys (mass fraction,%)

Samples	Cu	Ni	Fe	Mn	C	S	P
Cu-10.44Ni-0.84Fe	Bal	10.44	0.84	0.94	0.0040	＜0.0010	＜0.0010
Cu-10.52Ni-1.26Fe	Bal	10.52	1.26	0.95	0.0041	＜0.0010	＜0.0010
Cu-10.48Ni-1.76Fe	Bal	10.48	1.76	0.99	0.0037	＜0.0010	＜0.0010

2.2 Electrochemical measurement

The electrochemical measurements were conducted using an electrochemical workstation (CHI660E) in a conventional three-electrode cell. The potentials were referenced to a saturated

calomel electrode (SCE). A Pt sheet (20×20 mm) was used as the counter electrode. The electrochemical impedance spectroscopy (EIS) was carried out in a frequency ranging from 100 kHz to 10 mHz at open circuit potential (OCP) in a steady state.The potentiodynamic polarization curves were measured in the range of -500 mV to 100 mV with a scan rate of 1 mV/s. All tests were carried in a 3.5 % NaCl solution for one month at room temperature (~25 ^{o}C). Each electrochemical test was performed at least twice to confirm the reproducibility.

2.3 Surface corrosion product characterzation analysis

The characterization of corrosion product was analysed by X-ray Diffraction (XRD) and X-ray photoelectron spectroscopy (XPS). The XRD was run at PANalytical Xpert Powder diffract meter with Cu K_{α} radiation, operating at 40 kV and scanning from 10-90º. XPS spectra (EscaLab 250Xi) were recorded with Al Kα radiation (1486.6 eV) under vacuum (5×10^{-9} mbar).The C 1s peak located at 284.8 eV was used as a reference peak. The signals of surface corrosion product were collected after sputtering for 0, 50, 100, 150 and 200 nm. The spectra fitting was carried out using Avantage 5.52 software.

3. RESULTS AND DISCUSSION

3.1 Electrochemical measurement

3.1.1 EIS

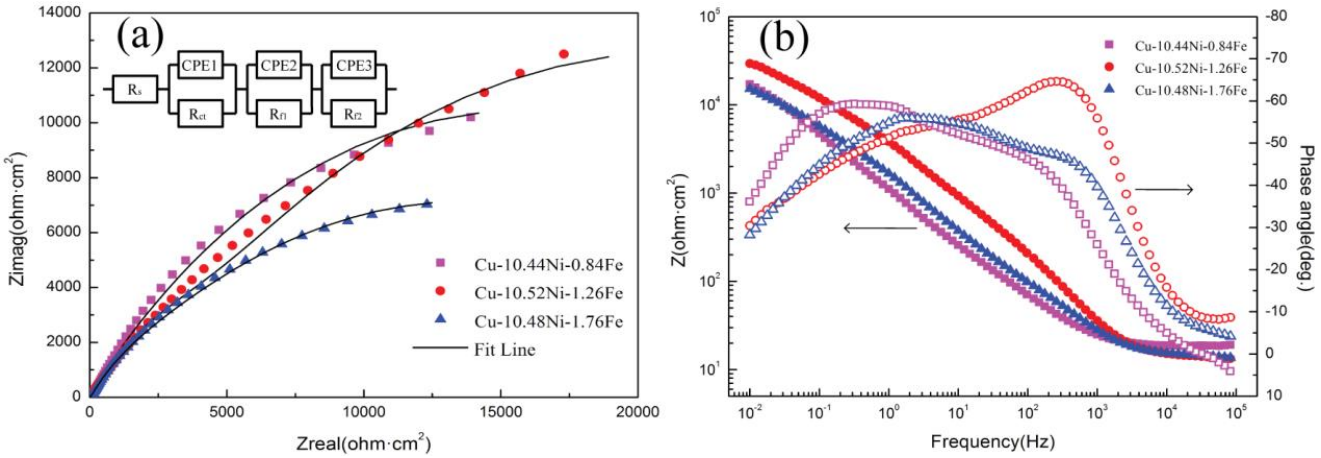

Figure 1. Nyquist plots (a) and Bode plots (b) of Cu-10Ni-Fe_x immersed in 3.5 % NaCl solution

Fig.1(a) and Fig.1(b) present the Nyquist plots and Bode plots results of Cu-10Ni-Fe_x alloys. It can be seen in Fig.1(a) that all the Nyquist plots show a semicircle arc. The radius of thesemicircle arc significantly differs among samples with different Fe. The radius of the plot measured on Cu-10.44Ni-0.84Fe is larger than that of the plots measured on other alloys at low frequency, whilst the radius of Cu-10.44Ni-1.26Fe is the largest at high frequency. The hollow and solid symbols shows in Fig.1(b)

represent the phase and impedance, respectively. The bode plots show that Cu-10.52Ni-1.26Fe exhibits higher impedance modulus value (|Z|) than the other sample at low frequency and a similar impedance modulus value (|Z|) at high frequency.

The experimental data had been fitted with several models of equivalent circuits. Using the equivalent circuit shown in the illustration of Fig. 1(a), the results with best fit between experiment and fitting were obtained. Therein, R_s, R_{ct}, R_{f1} and R_{f2} are defined as the solution resistance, charge transfer resistance and the resistance of corrosion product film, respectively; Q_1 is the constant phase element (CPE) of the electric double layer, and Q_2 and Q_3 are the CPE of the film. Considering the non-uniformity of the corrosion product on the surface of sample, CPEs were used to take the place of an ideal capacitance element. The impedance was calculated relating to the frequency as follows: $Z_{CPE} = Y^{-1}(j\omega)^{-n}$, where Y is the CPE magnitude, j is the imaginary unit, ω is the angular frequency and n is the CPE exponent[14,15]. The total resistance value, R_{total}, was calculated by taking the sum of the individual resistances using the following formula[13,16]:

$$R_{total} = R_{ct} + R_{f1} + R_{f2} \quad (1)$$

The curve-fitted results are presented in Table.2. Theoretically, the R_s values measured for different samples in the same solution should be similar and the R_s measured from Cu-10.44Ni-0.84Fe, Cu-10.52Ni-1.26Fe, Cu-10.48Ni-1.76Fe were similar with values of 17.94 Ω·cm^2, 13.20 Ω·cm^2, 13.46 Ω·cm^2, respectively. The R_{ct} values of samples were 59.57 Ω·cm^2, 250.4 Ω·cm^2, 21.34 Ω·cm^2 in turn ,while the R_{total} values were 30528.57 Ω·cm^2, 39857.40 Ω·cm^2, 25616.34 Ω·cm^2. The R_{ct} values and R_{total} of Cu-10Ni alloy with addition of 1.26 Fe were increased than other addition amount. This means that dissolution of metal on the surface was inhibited and a more protective product film was formed with addition of 1.26 Fe than other addition amount. The various of values were associated with the change of composition of the corrosion product film on the surface of the alloy.

Table 2. Circuit parameters fitted from the EIS result of Cu-10Ni-Fe$_x$ immersed in 3.5 % NaCl solution

		Q_1			Q_2			Q_3			
Sample	R_s	Y_0	n_1	$R_{ct.}$	Y_0	n_2	R_{f1}	Y_0	n_3	R_{f2}	R_{total}
Cu-10.44Ni-0.84Fe	17.94	0.000023	0.8011	59.57	0.000513	0.6646	3119	0.000419	0.8046	27350	30528.57
Cu-10.52Ni-1.26Fe	13.20	0.000028	0.9182	250.4	0.000078	0.8023	3977	0.000143	0.7730	35630	39857.40
Cu-10.48Ni-1.76Fe	13.46	0.000048	0.9676	21.34	0.000330	0.6825	2885	0.000317	0.6887	22710	25616.34

Units (R: Ωcm^2, Y: Ωs^{-1}cm^{-2}s^n)

3.1.2 Potentiodynamic polarization curves

Fig. 2 presents the potentiodynamic polarization curves of the Cu-10Ni-Fe$_x$ samples immersed in 3.5 % NaCl solution. One can fit the cathodic and anodic polarization curves by Tafel extrapolation to obtain the corrosion parameters[17,18]. The corrosion potential (E_{corr}), corrosion current density (I_{corr}) and Tafel slope (β_a and β_c) were calculated from the linear segments and the results are shown

in Table 3. Obviously, the E_{corr} of Cu-10.44Ni-0.84Fe, Cu-10.52Ni-1.26Fe, Cu-10.48Ni-1.76Fe are -392 mV, -291 mV, and -376 mV, respectively. Moreover, the i_{corr} was reduce from 0.407 μA·cm^{-2} of Cu-10.44Ni-0.84Fe to 0.206 μA·cm^{-2} of Cu-10.52Ni-1.26Fe after adding more Fe, and then the value increase to 0.976 μA·cm^{-2} of Cu-10.52Ni-1.76Fe. The anode Tafel slope (β_a) of Cu-10.52Ni-1.26Fe is 82 mV·dec^{-1}, which increases than that of other alloys. This means that dissolution resistance of the corrosion product film of Cu-10.52Ni-1.26Fe increases. Additionally, the I_{corr} can be converted by following formula[14] to obtain the corrosion rate and the values presented in the Table 3:

$$v(\frac{mm}{a}) = \frac{A \cdot I_{corr}}{n \cdot F \cdot \rho} \times 87600 \qquad (2)$$

where A is the molar mass of alloy, n is the charge transfer number of reactant, F is the Faraday constant and ρ is the density of the alloy.

Compared with the corrosion rate in Cu-10.48Ni-1.76Fe of 0.0113 mm/a, the corrosion rate of Cu-10.52Ni-1.26Fe has decreased to 0.0024 mm/a. As shown in Table 3, the corrosion rate of the corrosion rates are obeyed the sequence, Cu-10.52Ni-1.26Fe ＞ Cu-10.44Ni-0.84Fe ＞ Cu-10.48Ni-1.76Fe. It is clear that the minor change of iron content has a great influence on the corrosion resistance of Cu-10Ni alloy. All the results of the electrochemical measurements indicate that the Cu-10.52Ni-1.26Fe exhibits much superior corrosion resistance compared to the other samples.

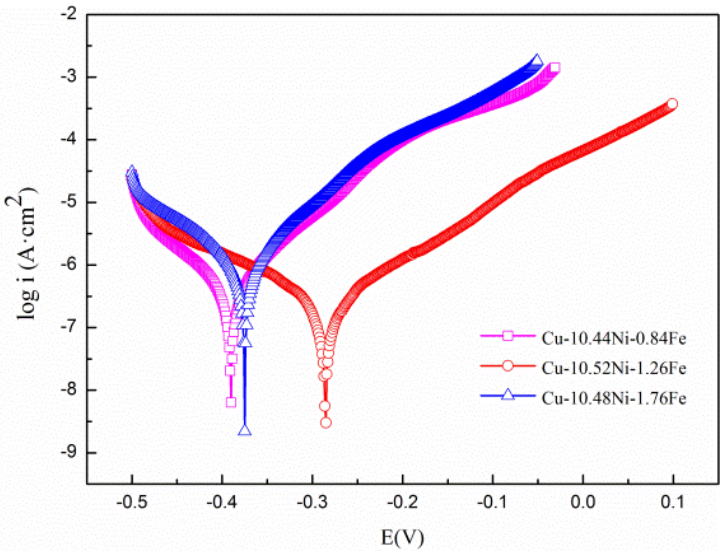

Figure 2. Potentiodynamic polarization curves of Cu-10Ni-Fe$_x$ immersed in 3.5 % NaCl solution

Table 3. Potentiodynamic polarization analysis data of Cu-10Ni-Fe$_x$ immersed in 3.5 % NaCl solution

Sample	E_{corr}/mV	i_{corr}/(μA·cm^{-2})	β_a / mV dec^{-1}	β_c / mV dec^{-1}	V/(mm/a)
Cu-10.44Ni-0.84Fe	-392	0.407	79	-68	0.0047
Cu-10.52Ni-1.26Fe	-291	0.206	82	-61	0.0024
Cu-10.48Ni-1.76Fe	-376	0.976	70.5	-56.7	0.0113

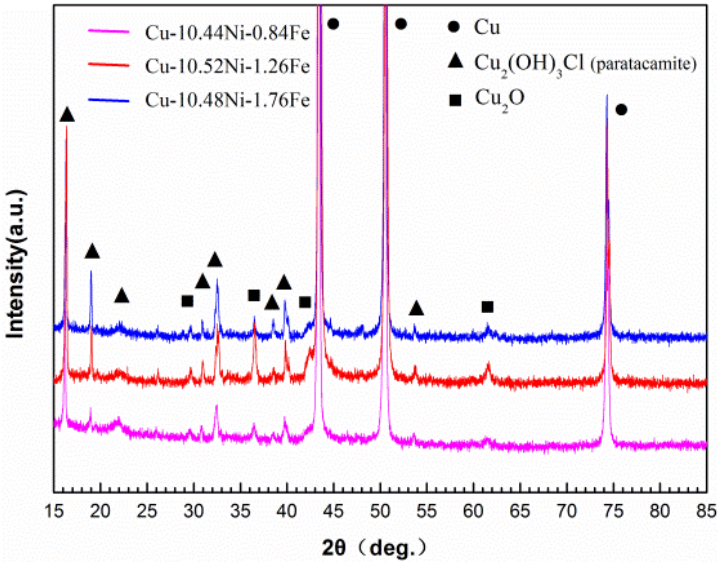

Figure 3. The XRD patterns of the corrosion product formed on the surface of Cu-10Ni-Fe_x immersed in 3.5 % NaCl solution

3.2 Surface analysis of corrosion product films

3.2.1XRD analysis

To better understand the influence of Fe on the corrosion product of Cu-10Ni alloys, XRD was used for the phase analysis of the corrosion products films on the alloy surface. The XRD pattern for the product film formed on the surface of the Cu-10Ni-Fe_x in 3.5 % NaCl solution are presented in Fig. 3. The presence of Cu_2O, $Cu_2(OH)_3Cl$ and Cu in the corrosion products was determined by marked characteristic peaks. No trace of iron or nickel compounds was found in the pattern.

The Cu peaks in the Fig.3 may come from portions of the substrate that were unprotected due to rupture of the corrosion product film during sample preparation or transport. During the immersion process, the copper preferentially dissolves due to the presence of Cl^- on the surface of the alloys and redeposits to form Cu_2O as show in the following reactions[19,20]:

$$Cu + 2Cl^- \leftrightarrow CuCl_2^- + e^- \quad (3)$$

$$CuCl_2^- + 2OH^- \leftrightarrow Cu_2O + H_2O + 4Cl^- \quad (4)$$

The $Cu_2(OH)_3Cl$ was formed by the Cu_2O reacting with Cl^- adsorbed on the surface of films by following reaction due to an increase of the thickness the Cu_2O film and a shift of the corrosion potential to a more positive value[21]:

$$Cu_2O + Cl^- + 2H_2O \leftrightarrow Cu_2(OH)_3Cl + H^+ + 2e^- \quad (5)$$

It is noteworthy that the $Cu_2(OH)_3Cl$ in the form of paratacamite. Frost reported that paratacamite is the most stable phase in the presence of substitution of Cu(II) by Ni(II) using Raman spectroscopy[20,22].

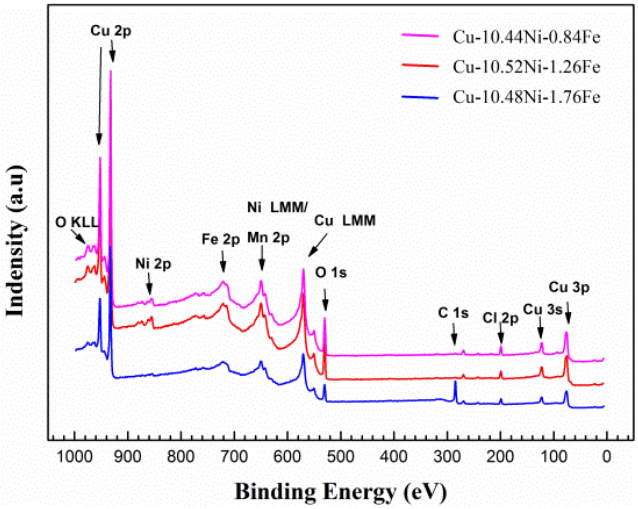

Figure 4. XPS survey spectra of the corrosion product on the surface of Cu-10Ni-Fe_x immersed in 3.5 % NaCl solution for one month after sputtering for 1000 s

3.2.2 XPS analysis

The XPS survey spectra of the corrosion product film formed on the surface of Cu-10Ni-Fe_x after sputtering for 1000 s are shown in Fig. 4. The elements of the film were similar and the films were composed of Cu, Ni, Fe, O, and Cl. Fig. 5 presents the survey spectra with different element depths for the corrosion product film on the surface of sample. The different symbols and colours showed in Fig. 5 represent the elements and samples, respectively. As seen from Fig. 5, the element content tends to stabilize after sputtering to 50 nm thickness. The content of Ni increased slightly with increasing depth of sputtering time, whilst the change of Cl and Cu were the opposite and content of O and Cu changed little. The Cu-10.52Ni-1.26Fe has the highest Ni content and lowest Cl and Cu content, whilst Cu-10.48Ni-1.76Fe has the opposite contents. At least 6 % of Cl^- can still be detected in the product film after sputtering for 1000 s, indicating that Cl^- has diffused into the inside of the film.

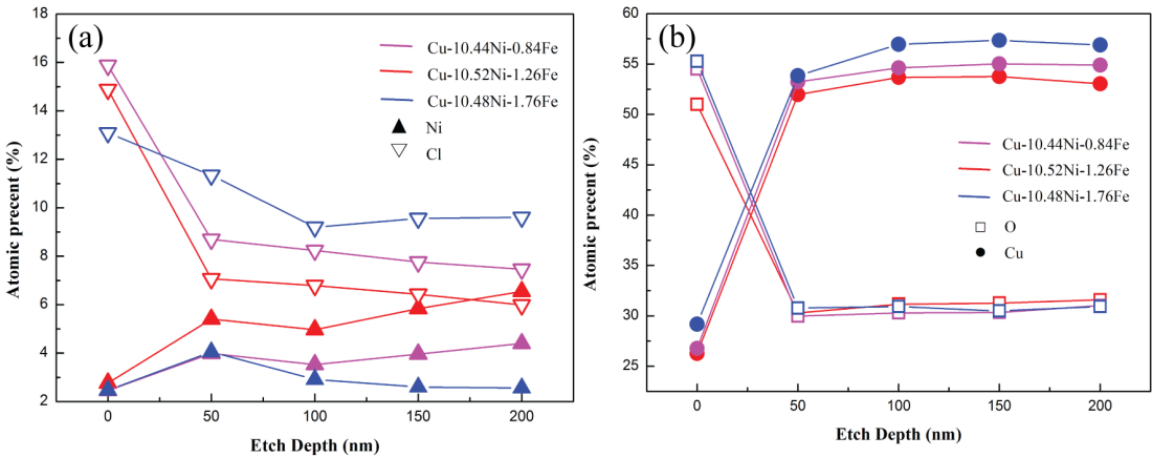

Figure 5. Depth profiles of elements for the samples with different element depth of the corrosion product on the surface of Cu-10Ni-Fe_x immersed in 3.5 % NaCl solution. (a) Ni and Cl elements, (b) Cu and O elements.

Fig. 6 and Fig. 7 present the high-resolution XPS spectra of Cu 2p and O 1s in the surface films after etching for 1000 s. Two distinct peaks can be found from Fig. 6 at the binding energy (B.E.) of 932.8 eV and 952.5 eV, corresponding to Cu/Cu_2O[23]. A weak peak can be found at the B.E. of 942.2 eV, corresponding to $Cu_2(OH)_3Cl$[20]. There was no observation of other compounds of Cu. It can be seen that the O 1s spectra showed in Fig. 7 are similar. The O 1s spectra of the film consisted of an intense peak at the B.E of 530.5 eV and two relatively weak peaks at B.E of 531.6 eV and 532.3 eV. Three peaks at the B.E. of 530.5 eV and 531.6 eV and 532.3 eV resulted from deconvolution of the core-level O 1s spectra,corresponding to O^{2-} and OH^- and hydrate water, respectively[24,25].

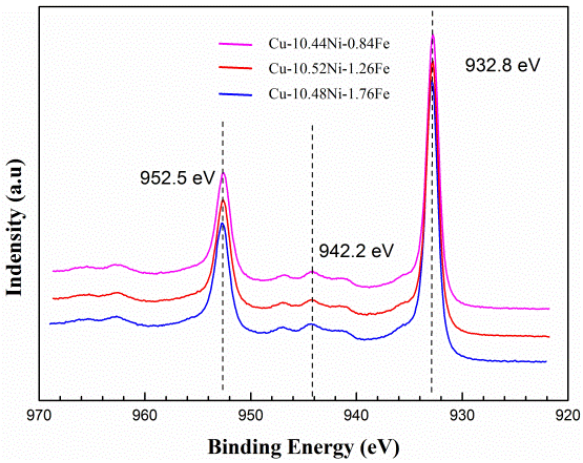

Figure 6. XPS spectra of Cu 2p collected from product film formed on the surface of Cu-10Ni-Fe_x immersed in 3.5 % NaCl solution

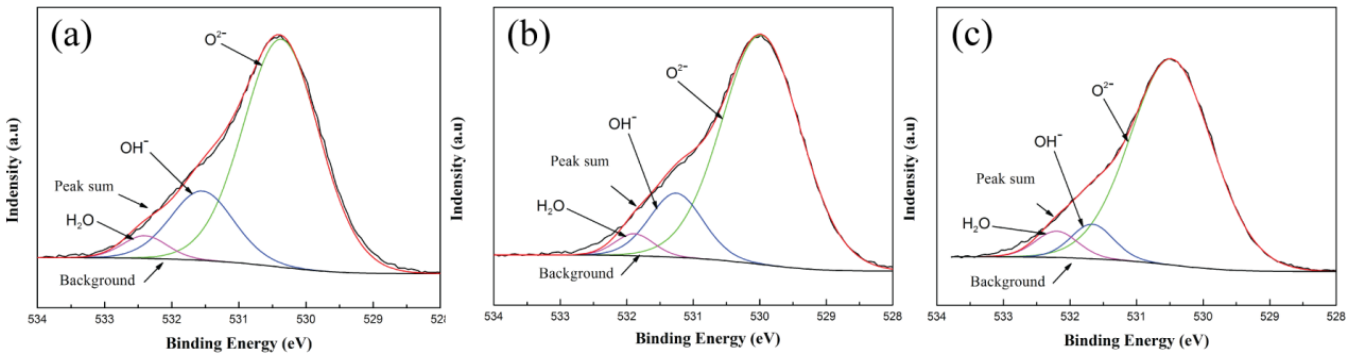

Figure 7. XPS spectra of O 1s collected from product film formed on the surface of Cu-10Ni-Fe_x immersed in 3.5 % NaCl solution. (a) Cu-10.44Ni-0.84Fe, (b) Cu-10.52Ni-1.26Fe, (c) Cu-10.48Ni-1.76Fe.

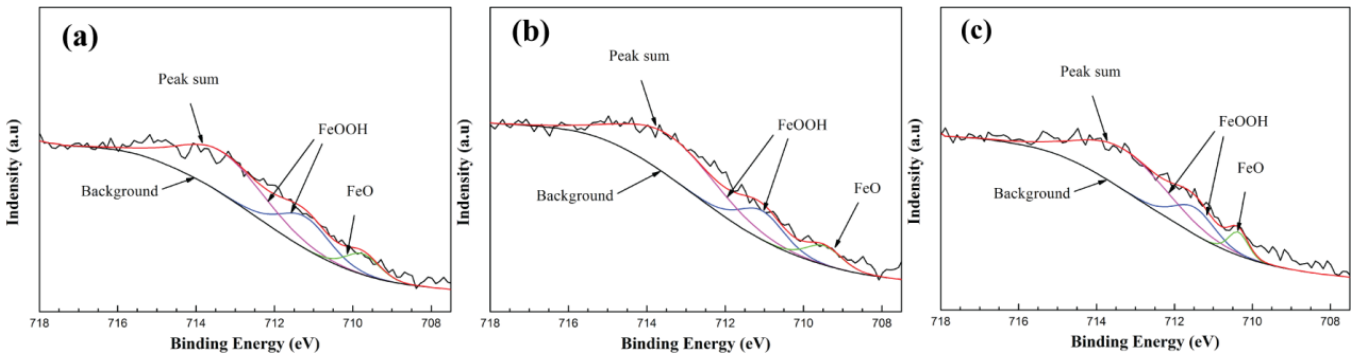

Figure 8. XPS spectra of Fe 2p Cu-10Ni-Fe_x immersed formed on the surface of Cu-10Ni-Fe_x immersed in 3.5 % NaCl solution. (a) Cu-10.44Ni-0.84Fe, (b) Cu-10.52Ni-1.26Fe, (c) Cu-10.48Ni-1.76Fe.

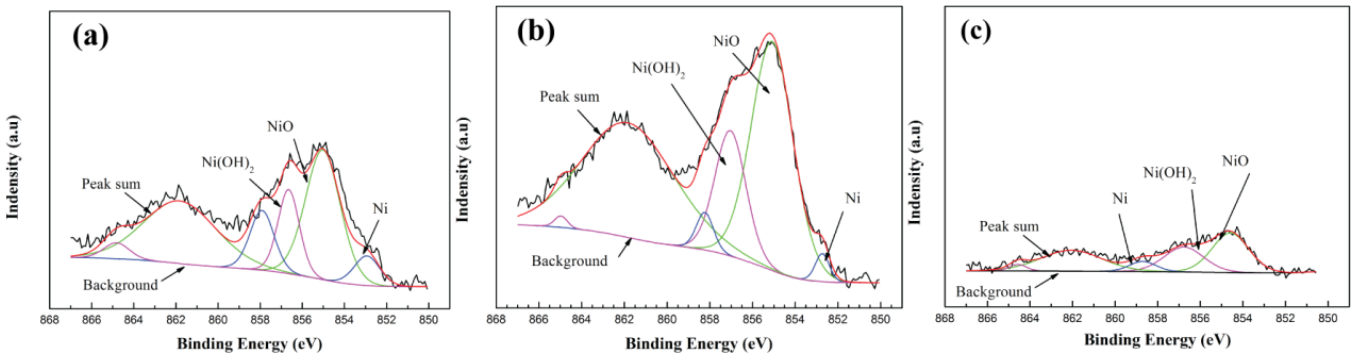

Figure 9. XPS spectra of Ni 2p Cu-10Ni-Fe_x immersed formed on the surface of Cu-10Ni-Fe_x immersed in 3.5 % NaCl solution. (a) Cu-10.44Ni-0.84Fe, (b) Cu-10.52Ni-1.26Fe, (c) Cu-10.48Ni-1.76Fe.

The XPS high-resolution spectra of Fe 2p of surface films after etching for 1000 s are presented in Fig. 8. Three distinct peaks at the 709.5 eV and 711.06 eV and 713.28 eV resulted from the deconvolution of the core-level Fe 2p spectrum, corresponding to FeOOH and FeO[26,27]. The relative quantities of Fe compounds fitting the Fig. 8 data on the corrosion product surface are presented in Table 4. As shown in table 4, Cu-10.52Ni-1.26Fe has the highest content of FeOOH and Cu-10.48Ni-1.76Fe has the lowest content of FeOOH.

Fig. 9 presents the high-resolution XPS spectra of Ni 2p of surface films after etching for 1000 s. Considering the double nature of Ni 2p lines at the peak fitting, the curves were fitted with similar binding energy separation (approximately 6eV) of the double peak, FWHM and intensity ratio [28]. The fitted results shown in Fig. 9 reveal that the XPS spectra of Ni 2p etch for 1000 s contained metallic Ni, NiO and $Ni(OH)_2$. The centre peak of metallic Ni is around 852.7 eV and shake-up peak is around 858.1 eV. The centre peak of NiO is around 855.9 eV and shake-up peak is around 861.9 eV. The centre peak and shake-up peak of $Ni(OH)_2$ are around 856.9 eV and 865.0 eV, respectively[23]. Table 4 shows the relative quantities of Ni compounds fitting the Fig. 9 data in the corrosion product

surface. Most Ni atoms exist in the form of oxidized NiO and $Ni(OH)_2$. The content and proportion of NiO were highest in Cu-10.52Ni-1.26Fe, corresponding to the best corrosion resistance. While Cu-10.48Ni-1.76Fe had the lowest content of NiO, corresponding to the worst corrosion resistance. The nature of the corrosion product film formed on the surface determines the corrosion resistance of Cu-10Ni-Fe_x alloy. In this investigation, the corrosion product film formed on the surface of on Cu-10.52Ni-1.26Fe displayed a better resistance than that of other samples. There is no doubt that this difference of resistance is attributed to the difference of Fe content in the alloys, which exhibits the following behaviours.

Table 4. Fitting parameters for XPS spectra and relative quantities in the corrosion product film of Cu-10Ni-Fe_x alloy immersed in 3.5 % NaCl solution

Valence state	Sample	Proposed compounds	Intensity (counts/s)	Relative quantity (%)
Fe	Cu-10.44Ni-0.84Fe	FeOOH	18645.41	87.61%
		FeO	2637.00	12.39%
	Cu-10.52Ni-1.26Fe	FeOOH	19528.29	88.28%
		FeO	2592.69	11.72%
	Cu-10.48Ni-1.76Fe	FeOOH	17885.25	89.79%
		FeO	2034.23	10.21%
Ni	Cu-10.44Ni-0.84Fe	Ni	8508.48	16.32%
		NiO	35107.98	67.32%
		$Ni(OH)_2$	8533.86	16.36%
	Cu-10.52Ni-1.26Fe	Ni	3904.8	4.11%
		NiO	75980.8	79.89%
		$Ni(OH)_2$	15217.3	16.00%
	Cu-10.48Ni-1.76Fe	Ni	1035.41	6.75%
		NiO	10323.73	67.25%
		$Ni(OH)_2$	3991.11	26.00%

3.3 Effect of Fe on corrosion product film

In general, copper alloys form a Cu_2O film which is main component of the corrosion product film on the surface during the corrosion process. According to the previous studies of N. Sato and the the point defect model (PDM)[29-31], Cu_2O is a p-type semiconductor and Cu^+ of Cu_2O dissolves into solution to form cation vacancies ($V_{Cu}^{'}$) after the formation of the film. The adsorbed O atom on the surface occupies a regular O site of the film and forms $V_{Cu}^{'}$ and electron holes ($h^{\cdot}$). The concentration of $V_{Cu}^{'}$ and $h^{\cdot}$ on the interface increases with time and generates a driving force which diffuses into the film. The metallic Fe and Ni of the substrate incorporate the $V_{Cu}^{'}$ after that shift to the interface

between substate and film by diffusion, resulting in the improvement of the corrosion resistance of the Cu_2O film.

The difference in iron content in the alloy ultimately leads to the difference in FeOOH in the corrosion product film.. The product film of the sample with 1.26 wt.% Fe contains more FeOOH, whilst the sample with 1.76 wt.% Fe contains less FeOOH. It is advantageous to maintain the amorphous structure in the product film when Fe exists as FeOOH[32]. The cross-linked structure composed of hydrate water and hydrogen bonds, which improve the corrosion resistance of the film. The increase of FeOOH inhibits the continued dissolution of Ni, which increases Ni content in the corrosion product film. Part of the Ni reacts with the dissolved hydrate water and oxygen in the product film to form $Ni(OH)_2$ and NiO. Ma believes that NiO exists in the amorphous in the corrosion product film[20]. FeOOH can maintain the amorphous structure in the product film, resulting in the highest NiO ratio of Cu-10.52Ni-1.26Fe. The thermodynamic stability of NiO is greater than that of Cu_2O and Cu^+ is more easily dissolved to form $V_{Cu}^{'}$ than Ni^{2+} , which improves the stability of the films[33]. When the proportion of NiO in the film increases, the ionic conductivity and electronic conductivity of the film layer decreases.

Furthermore, Cl^- is adsorbed on the surface of the film and then occupies the vacancies created by the O of the film (i.e., $V_O^{\cdot\cdot} + Cl^- \rightarrow Cl_O^{\cdot}$)[34,35]. Then, the Cl^-combines with cations in the film to form a soluble chloride (i.e., $Cu_2O + 4Cl^- + 2H^+ \rightarrow 2CuCl_2^- + H_2O$), which causes partial destruction of the product film[36,37]. Cl^- has a stronger adhesion ability in areas containing point defects than in areas without point defects[38] and the inner $V_{Cu}^{'}$ promotes the adsorption of Cl^-. Wei[38] proposed that the adsorption and incorporation of Cl^- can lead to the diffusion coefficient of $V_{Cu}^{'}$ increasing by up to 3 orders of magnitude. The transport properties of film are represented by the diffusion coefficient of $V_{Cu}^{'}$ which plays a opposite role with the corrosion resistance. The product film of the Cu-10Ni alloy with Fe content of 1.26 wt.% contained a higher content of Ni. Ni is more efficient than copper in quenching electron holes to incorporate the $V_{Cu}^{'}$. When $V_{Cu}^{'}$ is filled with Ni, it hinders the diffusion path of Cl^- in Cu_2O, which reduces the content of Cl^-, as shown in Fig.5.

4. CONCLUSIONS

The corrosion characteristic of Cu-10Ni-xFe alloys immersed in 3.5% NaCl were systematically analysed via various techniques. Three main conclusions are summarized below:

1) The electrochemical experiment results consistently reveal that the product film on Cu-10.52Ni- 1.26Fe exhibits a much superior corrosion resistance compared to that of the other samples and the order corrosion resistance is Cu-10.52Ni- 1.26Fe＞Cu-10.44Ni-0.84Fe＞Cu-10.48Ni-1.76Fe.

2) In the product films, Fe exists in the form of FeOOH and FeO, whilst Ni exists in the form of metallic Ni, NiO and $Ni(OH)_2$.

3) The corrosion products formed on Cu-10.52Ni-1.26Fe contain the maximum FeOOH content, which related to the increase of NiO content and responsible for the optimal corrosion resistance.

ACKNOWLEDGEMENTS
This study is financially supported by the National Key R&D Program of China (2016YFB0301400, 2016YFB0301401) and the National Natural Science Foundation of China (Grant no. 51504104).

References

1. F. Mansfeld, G. Liu, H. Xiao, C.H. Tsai and B.J. Little, *Corros. Sci*., 36 (1994) 2063.
2. A.M. Beccaria and J. Crousier, *Brit. Corros. J*., 24 (1989) 49.
3. P. Druska, H.H. Strehblow and S. Golledge, *Corros. Sci*., 38 (1996) 835.
4. R.F. North and M.J. Pryor, *Corros. Sci*., 10 (1970) 297.
5. C.L. Ma, Z. Li, Y.J. Li and P.Z. Zhao, Nonferrous Metal Materials for Marine Applications, Chemical Industry Press, (2017) Beijing,China.
6. Y.G. Zheng and A.L. Ma, Manual of Copper Alloy Corrosion for Marine Applications, Chemical Industry Press, (2017) Beijing,China.
7. K. Efird, *Corrosion*, 33 (1977) 347.
8. J.M. Popplewell, R.J. Hart and J.A. Ford, *Corros. Sci*., 13 (1973) 295.
9. J. Zhang, Q. Wang and Y. Wang, *Acta. Metall. Sin*., 45 (2009) 1390.
10. G.L. Bailey, *J. Inst. Metals*, 79(1951) 243.
11. C. Pearson, *Brit. Corros. J*, 7(1972) 61.
12. R.Zanoni, E. Traversa, G. Montesperelli and G. Gusmano, *Corrosion*, 48 (1992) 404.
13. O.O. Ekerenam, A.L. Ma, Y.G. Zheng and W. Emori, *J. Mater. Eng. Perform*., 26 (2017) 1701.
14. Q.Y. Zhou, J.B. Jiang, Q.D. Zhong, Y. Wang, K. Li and H.J. Liu, *J. Alloy. Compd*., 563 (2013) 171.
15. Q. Liu, Q.X. Ma, G.Q. Chen, X. Cao, S. Zhang, J.L. Pan, G. Zhang and Q.Y. Shi, *Corros. Sci.,* 138 (2018) 284.
16. B.G. Prakashaiah, D.V. Kumara, A.A. Pandith, A.N. Shetty and B. E. Amitha Rani, *Corros. Sci*., 136 (2018) 326.
17. A.D. King, N. Birbilis and J.R. Scully, *Electrochim. Acta*, 121 (2014) 394.
18. Z.M. Shi, M. Liu and A. Atrens, *Corros. Sci*., 52 (2010) 579.
19. G. Kear, B.D. Barker, K.R. Stokes and F.C. Walsh, *Electrochimi. Acta*, 52 (2007) 2343.
20. A.L. Ma, S.L. Jiang, Y.G. Zheng and W. Ke, *Corros. Sci*., 91 (2015) 245.
21. S.A. Campbell, G.J.W Radford, B.D. Barker and C.D.S. Tuck, *Corrosion*, 58 (2002) 57.
22. R.L. Frost, *Spectrochim. Acta* A, 59 (2003) 1195.
23. Q. Luo, Z.B. Qin, Z.Wu, B. Shen, L. Liu and W.B. Hu, *Corros Sci*., 138 (2018) 8.
24. W. Wu, X.Q. Cheng, H.X. Hou, B. Liu and X.G. Li, *Appl. Surf. Sci*., 436 (2018) 80.
25. X. Leng, Y.D. Zhang, Q.Y. Zhou, Y.H. Zhang, Z.G. Wang, H. Wang and B. Yang, *Mater. Res. Express*., 5 (2018) 056513
26. J. Tang, Z.J. Wang and X.H. Xu, *Environm. Sci*., 34 (2013) 2650.
27. H. Luo, Z.M. Li, A.M. Mingers and D. Raabe, *Corros. Sci.*, 134 (2018) 131.
28. S. Colin, E. Beche, R. Berjoan, H. Jolibois and A. Chambaudet, *Corros. Sci.,* 41 (1999) 1051.
29. N. Sato, *Corrosion*, 45 (1989) 154.
30. D.D. Macdonald and A. Sun, *Electrochim. Acta*, 51 (2006) 1767.
31. D.D. Macdonald, *Electrochim. Acta*, 56 (2011) 1761.
32. C.J. Lin, Y. Mao and S.W. Tian, *J. Chin. Soc. Corros. Prot.,* 12 (1992) 205.
33. Z.Q. Cao, Y. Niu and W.T. Wu, *Rare. Metal. Mat. Eng.,* 34 (2005) 643.
34. Y.C. Zhang, M. Urquidi-Macdonald, G.R. Engelhardt and D.D. Macdonald, *Electrochim. Acta*, 69 (2012) 1.
35. W.H. Miao, Z.M. Gao and W.B. Hu, *Int. J. Electrochem. Sci*., 13 (2018) 771.
36. H. Strandberg and L.G. Johansson, *J. Electrochem. Soc*., 145 (1998) 1093.
37. M. Drogowska, L. Brossard and H. Ménard, *J. Electrochem. Soc*., 140 (1993) 1247.

38. X. Wei, C.F. Dong, P. Yi, A. Xu, Z.H. Chen and X.G. Li, *Corros. Sci*., 136 (2018) 119.